The physics of pandemics with application to COVID19

Stephen Miller (stephen.miller@unine.ch)
University of Neuchâtel https://orcid.org/0000-0003-2229-4073
Thanushika Gunatilake
University of Neuchâtel

Article

Keywords: propagation models, SEIR, ABM, COVID-19, Epidemic Type Aftershock Sequence

Posted Date: February 6th, 2021

DOI: https://doi.org/10.21203/rs.3.rs-208944/v1

The physics of pandemics with application to COVID19

Thanushika Gunatilake and Stephen A. Miller

Abstract

Numerous models exist with the goal of modeling the propagation of COVID-19 and other epidemics or pandemics. These models include the SEIR (Susceptible-Exposed-Infected-Removed) model [1, 2], Agent Based Models (ABM) [3, 4, 5], and continuum models of reaction diffusion [6, 7]. Each of these modelling approaches contain multiple and sometimes intractable variables [2, 8], resulting in large uncertainties in outcomes, thus restricting their utility in guiding local, national, and international governmental decisions for managing and controlling pandemics. There exists a need for a simple, fast, deterministic, scalable, and accurate model that captures the dominant physics of pandemic propagation. Here we propose such a model by adapting a physical earthquake/aftershock model [9] to the COVID19 problem. The aftershock model revealed the physical basis for the Epidemic Type Aftershock Sequence (ETAS) model [10, 11] as a highly non-linear diffusion process, thus permitting a grafting of the underlying physical equations into a formulation for calculating infection pressure propagation in a pandemic-type model. Model results show excellent correlations with observed infection rates for all cases studied to date. In alphabetical order, these include Austria, Belgium, Brazil, France, Germany, Italy, Melbourne (AU), New Zealand, Spain, Sweden, Switzerland, UK, and the USA. Importantly, the model is predominantly controlled by one parameter (α), which modulates societal compliance to governmental actions. We find that differing societal compliance between countries results in dramatically different outcomes given similar infection sources. These results provide an intuition-based approach to designing and implementing mitigation measures, with predictive capabilities for various mitigation scenarios.

1 Introduction

The global COVID19 pandemic demonstrated that modelling plays and essential role in managing and mitigating its spread and containment [12]. Modelling pandemics falls into roughly three categories; (1) the widely-used SEIR model [13], or many of its variations [14, 15], couples sets of ordinary differential equations constrained by numerous variables including the important (but difficult to constrain [8]) infection rate (R) to produce predictive outcomes; (2) ABM models numerically track up to 6.5 billion numerical people interacting with, and infecting, other numerical people based on (uncertain) rules of human-behaviour [16, 17]; and (3) Models of reaction-diffusion [18]. Other approaches include concepts of Self-Organized Criticality (SOC) [19] or Monte-Carlo simulations [20]. Each of these approaches have advantages and drawbacks, but all of these approaches are complex and thus of limited practical utility.

Here we adapt a simple model [9] of non-linear fluid pressure diffusion through a porous media to the COVID19 problem. The aftershock model revealed the underlying mechanism driving the empirical Omori-Utsu Law of aftershocks [21, 22], and the often-used statistical ETAS model. Since ETAS is by definition an epidemic model, and pandemics are simply large-scale epidemics, the physical aftershock model is an epidemic/pandemic model. Hence, the physics can be adapted and applied to epidemiological problems.

2 Physical Model

Diffusion of fluid pressure in a porous medium is governed by:

$$\frac{dP}{dt} = \frac{1}{\phi\beta} \bigtriangledown \cdot \left[\frac{k}{\eta} \bigtriangledown P \right] + \frac{Q}{\phi\beta} \tag{1}$$

where P is fluid pressure [Pa] above hydrostatic, t is time [s], ϕ is porosity [ ], β is compressibility $[Pa^{-1}]$, k is the permeability $[m^2]$, η is fluid viscosity [Pa s], and Q is a source term $[s^{-1}]$.
In the pandemic analogy, we apply an infection source rate (S_i), and calculate the time evolution of infection pressure (P_i) as it diffuses through societies. The pandemic model is thus:

$$\frac{dP_i}{dt} = \frac{1}{\phi\beta} \bigtriangledown \cdot \left[\frac{k_i}{\eta} \bigtriangledown P_i \right] + \frac{S_i}{\phi\beta} \tag{2}$$

where P_i is infection pressure [Pa], t is time [s], ϕ is a measure of the population distribution [ ], β is compressibility $[Pa^{-1}]$ interpreted as societal compliance, k_i is the infection permeability $[m^2]$ reflecting the resistance to infection pressure gradients, η [Pa s] is the viscous term describing the ease of flow (e.g. internal friction) via public transportation, geographical barriers, and frictional interaction between people, and S_i $[s^{-1}]$ is the infection source rate. We purposely preserve, for clarity, the physical units of the porous media analogy, however, we recognize the difficulty in quantifying infection pressure.

We further define the permeability as:

$$k_i = k_0 e^{\pm\alpha t} \tag{3}$$

where k_0 $[m^2]$ is the initial resistance to infection diffusion. A reduction in k_0 over a timescale α $[s^{-1}]$ reflects the increased resistance to flow in response to mitigation measures.

The source term S_i is defined in similar way:

$$S_i = Q_0 e^{\pm\alpha t} \tag{4}$$

where Q_0 $[s^{-1}]$ is introduced throughout the domain, initially concentrated at airports and ports of entry, and the same α as used in Equation 3 reflects the reduction of infection pressure sources because of mitigation measures.
We use the same α in Equations 3, 4 because it modulates the system compliance $\phi\beta$ in both the diffusion and source terms, and dominates the model behavior. The sign and value of α $[s^{-1}]$ is constrained by the data. Conceptually we might decompose β into political compliance β_p and economic compliance β_e because a country's economic health might also affect a country's response. Porosity is defined as $\phi = 0.5 - \left(\frac{f_s}{f_c}\right)$, where f_s is the population of a state and f_c is the population of the

entire country, and limits the range of ϕ to the model's geological analog. In this study, the data shows $0.2 < \phi < 0.49$ (see Supplemental Table 1 for information sources). Supplemental Table 1 also lists the source of our input for the viscous term η, which we equate to the use of public transportation and thus the probability of human interaction.

The model is divided into different domains defined by either states within each country, or neighborhoods with a city (e.g. Melbourne). We numerically solve, using implicit finite differences, the non-linear diffusion Equation 2 on a regular grid of 300x300 nodal points to calculate infection pressure and triggered infections across the named countries. No-flow boundary conditions are applied along all boundaries. Model infections occur when a nodal point reaches a defined pressure threshold, which is arbitrary, but set to 1 MPa for all countries, excepting those with initially sluggish testing protocols that required a slightly higher initial threshold. To allow multiple infections at the same nodal point, we double the threshold necessary to trigger each subsequent infection. We impose no inherent randomness in the model, however, the different characteristics of each country result in an inherent heterogeneity.

3 Data and Simulation Input

Figure 1 shows the number of reported cases normalized by the maximum reported cases for each data set over 300 days for Austria, Belgium, Brazil, France, Germany, Italy, Melbourne (AU), New Zealand, Spain, Sweden, Switzerland, UK, and the USA. The data is published by the European Centre for Disease Prevention and Control (ECDC) [23], which monitors the COVID19 pandemic. The Melbourne data was obtained from the Australian government of health and human services [24].

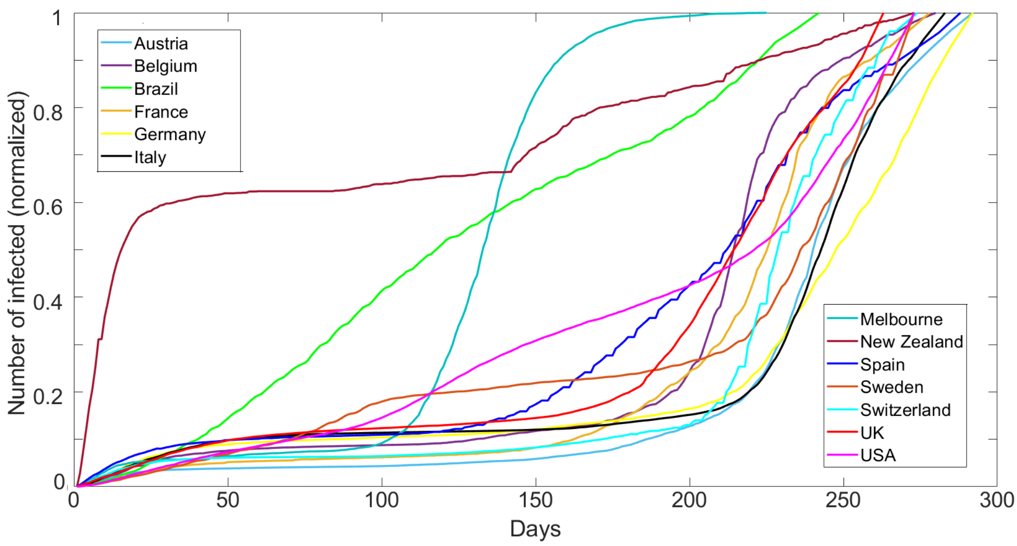

Figure 1: Compilation of cumulative infections for cases studied and shown in the Legend (Source: ECDC and Australian Government).

The data shows a very broad range of behavior, which we show below to be modelled only by varying α. For each simulation, we defined parameters ϕ, k, η, and Q, for each state within that country. These parameters are somewhat difficult to quantify, although straight-forward to qualitatively constrain, so we intentionally limit their range. The initial permeability k_0 takes on values of either $10^{-12}m^2$ or $10^{-13}m^2$, with the former applied to high population density and their corresponding transportation networks, and the latter for sparsely populated regions. The viscous term (η) takes on values of 10^{-3} or 10^{-2} $[Pa\, s]$ with the lower value reflecting the degree of public transport use. Finally, Q is $10^{-8}[s^{-1}]$ at points of entry and $10^{-9}[s^{-1}]$ throughout the remainder of the domain and is mostly the same on average for all studies cases (Supplementary Figure 3). These values were chosen to mirror (to some degree) their geological analog, and interestingly, the initial values best-suited for this model of infection pressure propagation have the hydraulic properties of water and beach sand as their porous media counterpart.

4 Results

From this input, the initial conditions at the start of each simulation (Figure 2 a) are heterogeneous and approximate at a large scale the overall societal setup. We use a timestep of one day, which results in a total simulation time of about 2 minutes on a typical laptop running a MATLAB script. (We also tested timesteps of 430 seconds, with no change in results). Our comparisons with data extend to almost 300 days, which covers the onset of the pandemic in each country until the both virus mutations and the introduction of vaccines modify the datasets in yet unknown ways.

Figures 2b-c show typical model results for four different countries (see Supplemental Figures 1 and 2 for the remaining cases). The calculated infection pressure concentrates in large urban areas (Figure 2 b), reflecting high population density and ease of flow (e.g. viscosity) but also shows pervasive elevated pressures throughout each country. This figure visualises the dramatic differences in infection pressure (and thus modelled infections) for the different countries. Unsurprisingly, the calculated number of repeat infections also correlates with population concentration and ease of flow (Figure 2 c).

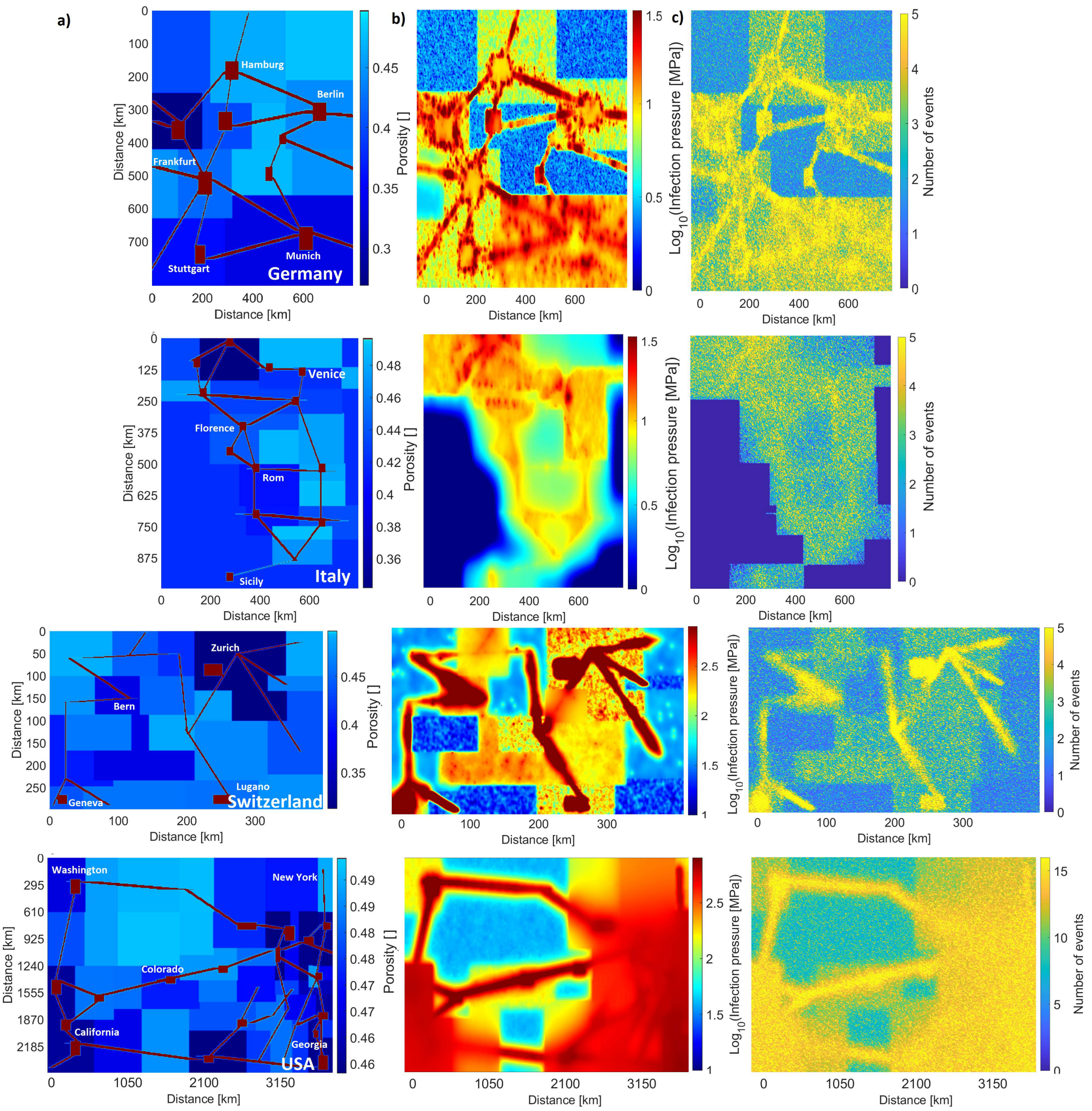

Figure 2: a) Model setup for Germany, Italy, Switzerland and the USA showing the source locations (red) signifying airports and intercity rail lines, and the various shades of blue scale with population density and delineate federal states. b) Calculated infection pressure at the end of the simulation. Note change in scale bar for each country. c) The number of repeated infections calculated in the model highlights the most affected regions and shows how elevated infection pressures (Figure 2b) continue to generate model infections.

Figure 3 shows the observed cumulative infections (i.e. Figure 1) superposed with modelled cumulative infections for all countries studied. Excellent agreement between model and observations is found for all countries, and model scaling is demonstrated by comparing results with observations at the local scale of Melbourne Australia. This agreement is observed despite the vast differences in governmental and societal response, and importantly, good agreement is achieved by modifying the parameter α, with different values for α chosen to fit the dynamics of COVID19 propagation (Figure 3 a). The parameter α dominates the model behavior because it modulates the system compliance $\phi\beta$ that appears in both the diffusion and source terms in Equation (2).

The best way to demonstrate the versatility of this model is to compare two end-member cases, Switzerland (Figure 3 l) and USA (Figure 3 n). The USA did not react to the oncoming pandemic, while Switzerland learned quickly from neighboring Italy that early and drastic measures were needed. Moreover, societal acceptance of governmental prevention strategies determines the efficacy of mitigation measures. In this model, these diverse societal reactions can be qualitatively constrained by the compressibility β (i.e. compliance) of these two systems. For example, both the USA and Switzerland have comparable economic opportunity, but in reaction to COVID19, they behaved in dramatically different ways to the same pandemic. Switzerland imposed strict and enforced shutdowns, mask requirements, and social distancing, etc, while the USA was late in reacting and mitigation measures were not strictly adhered to. In our model, that means that Switzerland was politically compliant ($\beta = 10^{-8}\ Pa^{-1}$) while the USA was relative politically stiff ($\beta = 7x10^{-9}\ Pa^{-1}$). We used $\beta = 10^{-8}Pa^{-1}$ for most simulations, however, a lower compliance $\beta = 7x10^{-9}Pa^{-1}$ was necessary for adequate fits to the data for Brazil, France, the UK, and the USA. Furthermore, Switzerland's mitigation directives were followed, resulting in quick recovery times for first wave (e.g. $1/\alpha \approx 7$days), while in the USA mitigation directives were either weak or not followed, resulting in very long recovery times (e.g. $1/\alpha \approx 100$ days).

The diffusivity reflects the rate of infection pressure propagation throughout each country. For intuitive reference the diffusivity of water and beach sand is 10-15 $[m^2s^{-1}]$, so from a physics perspective, the virus propagates very quickly. Parameter evolution (Figure 4) shows time histories of calculated infection pressure P_i and diffusivity κ, where $\kappa = \frac{k_0 e^{\pm\alpha t}}{\eta\phi\beta}$, for all cases studied. The initial rapid drops in diffusivity reflect pro-active societal response to government measures (e.g. EU countries and Switzerland), while diffusivity remains high (and thus the virus continues propagating) in Brazil, Sweden, and USA. Reduced diffusivity consequently results in rising infection pressure and pressure gradients, which remain in the system, to then subsequently diffuse upon relaxation of mitigation measures. This results in the onset of the 2^{nd} wave, which we model by imposing $-\alpha_2$ that dramatically increases diffusivity and the consequent reduction in P_i. Finally, α_3 reflects additional mitigation measures, and subsequent waves can be modelled with additional values for α.

Figure 5 quantifies the values for α, plotted for intuitive convenience as $1/\alpha$ [days], used in the simulations to fit the data (e.g. Figure 3), and a few important points stand out. First, Brazil and Sweden reveal the longest recovery times $1/\alpha_1$, indicative of lax if any mitigation measures. Similarly, the USA and the UK (and to some extent France) initially ignored the pandemic onset and this is also reflected by long recovery times. The remaining EU countries (and Switzerland) all imposed similar mitigation measures, and modelling shows recovery times of less than 2 weeks. The fastest recovery times were observed for Austria, New Zealand and Melbourne because of drastic and harsh lockdown requirements. The acceleration in infections at the onset of the 2^{nd} wave is quantified by $-1/\alpha_2$, and shows rapid acceleration in Belgium, USA, Spain, Switzerland, and the UK. This acceleration during the second wave is explained in the model as the onset of diffusion (instigated by relaxation of mitigation measures) of latent infection pressure gradients stored in the system. Finally, α_3 reflects the ongoing situation, and may change depending on governmental measures and societal response.

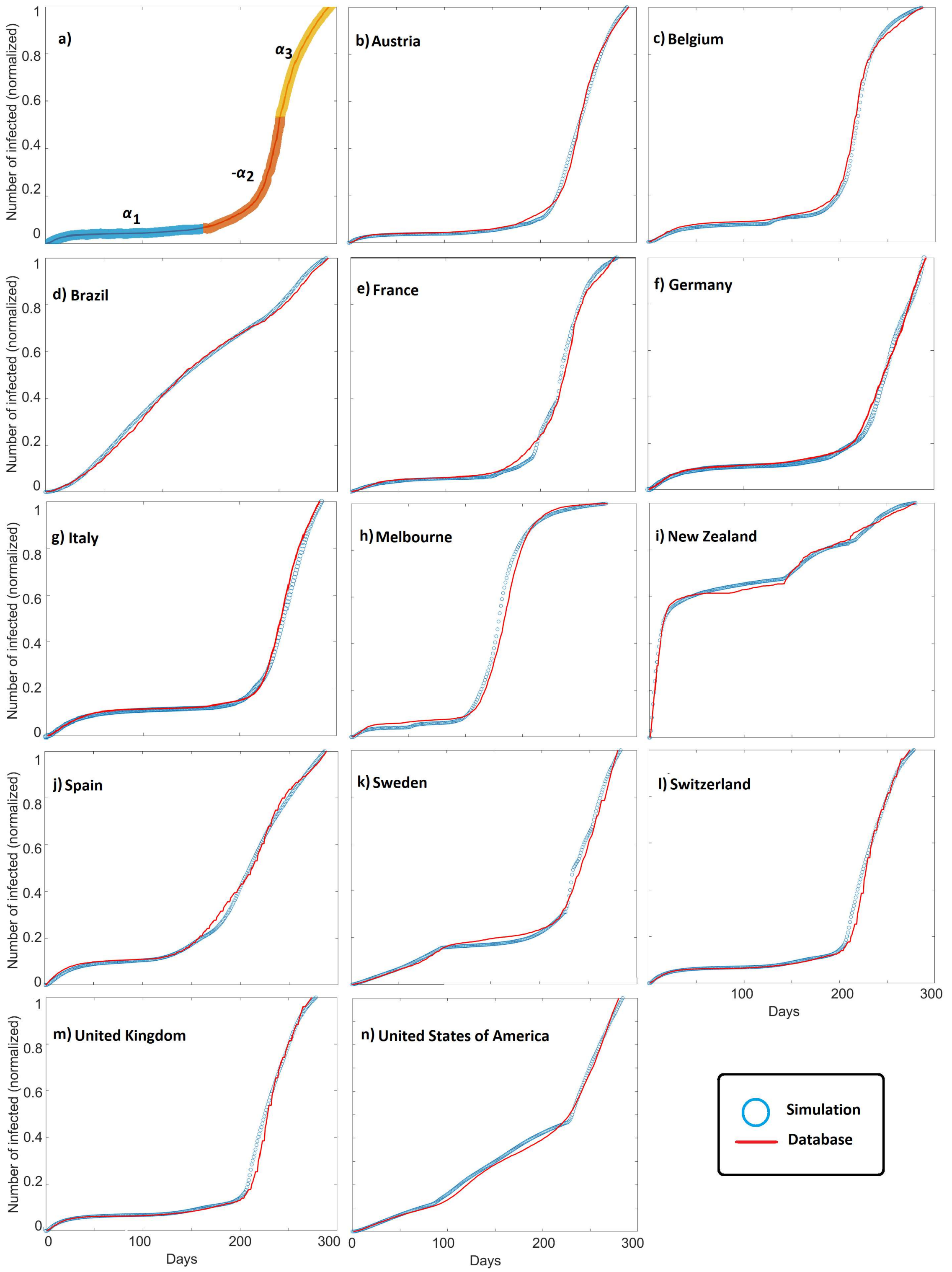

Figure 3: Comparison of data and model results for all data in Figure 1. The determination of $\pm\alpha$ is constrained by the data and demonstrated in Figure 3a.

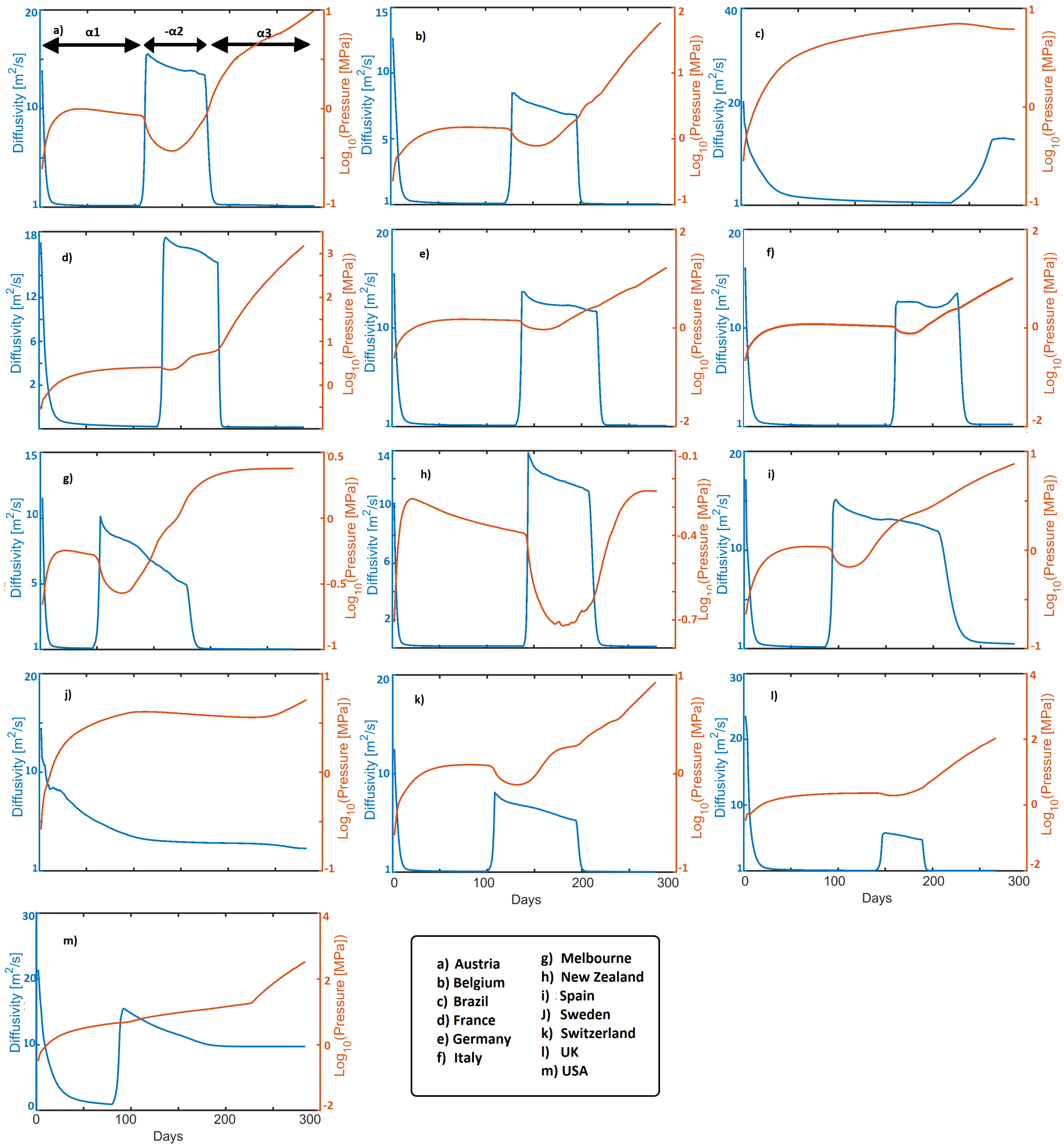

Figure 4: Modelled diffusivity and pressure time histories for triggered infection sites for each individual country and Melbourne. Looking at a typical EU result (i.e. Austria), the diffusivity initially decreases because of α Equation (3), reducing to between 2 and 4 $[m^2 s^{-1}]$ in response to mitigation efforts. Meanwhile, pressure increases over this timescale because of α in Equation (4), and is also diffusing resulting in mild pressure decreases. A sudden rise in κ correlates with imposition α_2, and thus the consequent pressure drop, followed by a mild apparent reduction in κ. This apparent reduction is caused by incorporating additional infection sites into the averaging, which include regions of lower permeability. Imposition of α_3 correlates with mitigation efforts that again reduce κ and increase P_i.

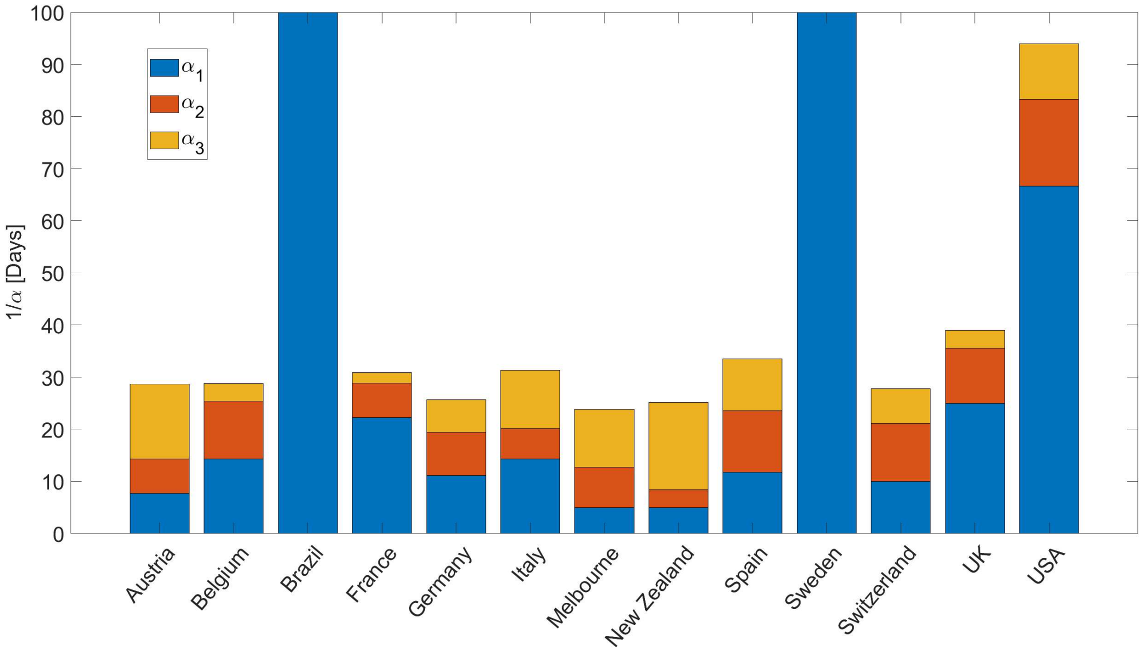

Figure 5: Summary of α values used in the simulations (See Figure 3a) showing long (initial) recovery times (α_1) for countries with few initial mitigation measures (e.g. Brazil, Sweden, USA), and to some extent France and the UK. All other countries and Melbourne show similar recovery times in response to swift and similar mitigation measures. The second wave ($-\alpha_2$) shows similar behavior between countries with slight variations, while α_3 is still ongoing. Note that the concavity for New Zealand at the onset of the second wave (Figure 3i) required $+\alpha_2$, and that Sweden and Brazil had essentially no recovery from the first wave, so α_2 and α_3 are essentially zero.

5 Discussion and Conclusions

We presented a simple model for the propagation of infection pressure through societies and compared model results with global COVID19 data. We find excellent agreement for all cases studied, and importantly, fits to the data are achieved by varying parameter α, where α quantifies the response to mitigation efforts. We also propose correlating β with societal constraints, in particular societal compliance. The data indicated that β was country-dependent, with containment of the virus observed in socially compliant countries that responded positively to benign authority and expert directives. On the contrary, socially stiff countries where trust in government is limited or self-survival prevails, similar infection pressures result in much worse outcomes. These intuitively obvious results backed by a quantitative model may allow governmental policy decisions to predict likely outcomes.

The result that only slight variations in model parameters can reproduce all observations of infection rates across the globe strongly indicates that this model captures the essence of the physics of pandemics. This deterministic model has predictive capabilities because once calibrated against the historical record (anywhere in its history), the model can be explored to project likely outcomes for different mitigation scenarios. The influence of vaccines and mutations can be addressed in future modeling. Finally, the model suggests that future strategies should be explored for reducing the latent infection pressure remaining in societies after successful mitigation measures.

References

[1] Carcione, J. M., Santos, J. E., Bagaini, C. & Ba, J. A simulation of a covid-19 epidemic based on a deterministic seir model. *Frontiers in public health* **8**, 230 (2020).

[2] Thompson, R. N. *et al.* Key questions for modelling covid-19 exit strategies. *Proceedings of the Royal Society B* **287**, 20201405 (2020).

[3] Gharakhanlou, N. M. & Hooshangi, N. Spatio-temporal simulation of the novel coronavirus (covid-19) outbreak using the agent-based modeling approach (case study: Urmia, iran). *Informatics in Medicine Unlocked* **20**, 100403 (2020).

[4] Gilbert, N. & Bankes, S. Platforms and methods for agent-based modeling. *Proceedings of the National Academy of Sciences* **99**, 7197–7198 (2002).

[5] Silva, P. C. *et al.* Covid-abs: An agent-based model of covid-19 epidemic to simulate health and economic effects of social distancing interventions. *Chaos, Solitons & Fractals* **139**, 110088 (2020).

[6] Fisher, R. A. The wave of advance of advantageous genes. *Annals of eugenics* **7**, 355–369 (1937).

[7] Viguerie, A. *et al.* Diffusion–reaction compartmental models formulated in a continuum mechanics framework: application to covid-19, mathematical analysis, and numerical study. *Computational Mechanics* **66**, 1131–1152 (2020).

[8] Vespignani, A. *et al.* Modelling covid-19. *Nature Reviews Physics* **2**, 279–281 (2020).

[9] Miller, S. A. Aftershocks are fluid-driven and decay rates controlled by permeability dynamics. *Nature communications* **11**, 1–11 (2020).

[10] Ogata, Y., Matsu'ura, R. S. & Katsura, K. Fast likelihood computation of epidemic type aftershock-sequence model. *Geophysical research letters* **20**, 2143–2146 (1993).

[11] Helmstetter, A. & Sornette, D. Predictability in the epidemic-type aftershock sequence model of interacting triggered seismicity. *Journal of Geophysical Research: Solid Earth* **108** (2003).

[12] Holmdahl, I. & Buckee, C. Wrong but useful—what covid-19 epidemiologic models can and cannot tell us. *New England Journal of Medicine* **383**, 303–305 (2020).

[13] Li, M. Y. & Muldowney, J. S. Global stability for the seir model in epidemiology. *Mathematical biosciences* **125**, 155–164 (1995).

[14] Mwalili, S., Kimathi, M., Ojiambo, V., Gathungu, D. & Mbogo, R. Seir model for covid-19 dynamics incorporating the environment and social distancing. *BMC Research Notes* **13**, 1–5 (2020).

[15] Adiga, A. *et al.* Mathematical models for covid-19 pandemic: a comparative analysis. *Journal of the Indian Institute of Science* 1–15 (2020).

[16] Makarov, V., Bakhtizin, A., Sushko, E. & Sushko, G. A design system for scalable agent-based models with multi-stage interactions of agents forming social connections. *Lobachevskii Journal of Mathematics* **41**, 1492–1501 (2020).

[17] Batty, M., Crooks, A. T., See, L. M. & Heppenstall, A. J. Perspectives on agent-based models and geographical systems. In *Agent-based models of geographical systems*, 1–15 (Springer, 2012).

[18] Nauman Ahmed, M. R. e. a. Positive explicit and implicit computational techniques for reaction–diffusion epidemic model of dengue disease dynamics. *Advances in Difference Equations* **202** (2020).

[19] Contoyiannis, Y. *et al.* A universal physics-based model describing covid-19 dynamics in europe. *International Journal of Environmental Research and Public Health* **17**, 6525 (2020).

[20] Xie, G. A novel monte carlo simulation procedure for modelling covid-19 spread over time. *Scientific reports* **10**, 1–9 (2020).

[21] Omori, F. On the after-shocks of earthquakes. *J. Coll. Sci., Imp. Univ., Japan* **7**, 111–200 (1894).

[22] Utsu, T. A statistical study on the occurrence of aftershocks. *Geophys. Mag.* **30**, 521–605 (1961).

[23] ECDC. European centre for disease prevention and control - an agency of the european union. https://www.ecdc.europa.eu/en/covid-19/data. Online; accessed 31 January 2021.

[24] DHHS. Department of health and human services - victorian coronavirus (covid-19) data. https://www.dhhs.vic.gov.au/victorian-coronavirus-covid-19-data. Online; accessed 31 January 2021.

Figures

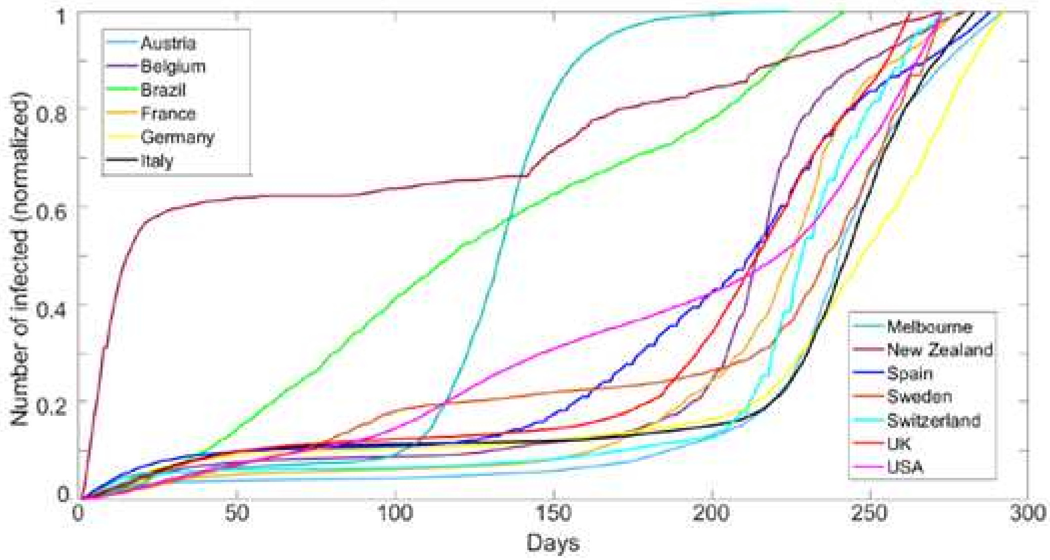

Figure 1

Compilation of cumulative infections for cases studied and shown in the Legend (Source: ECDC and Australian Government).

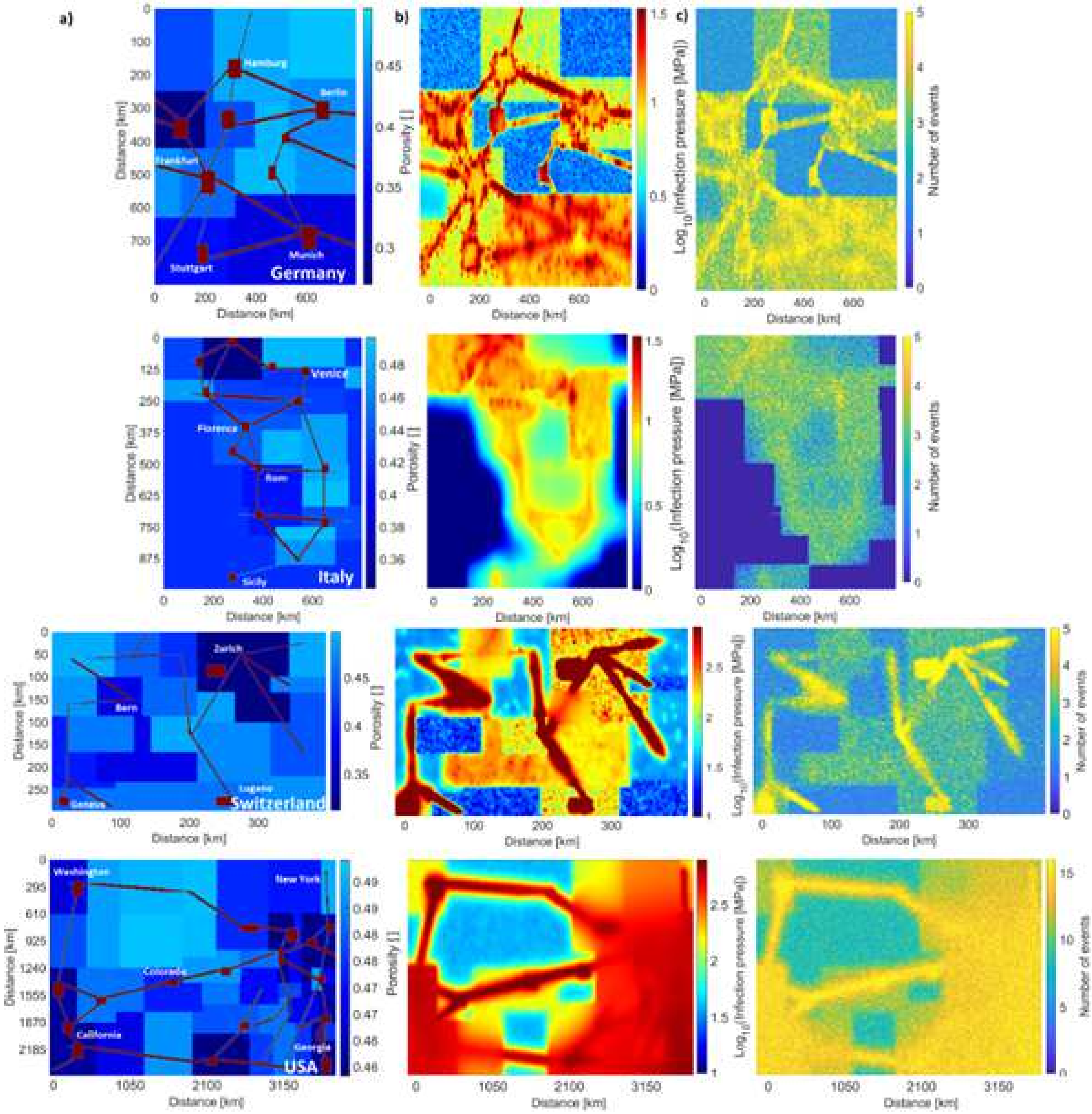

Figure 2

a) Model setup for Germany, Italy, Switzerland and the USA showing the source locations (red) signifying airports and intercity rail lines, and the various shades of blue scale with population density and delineate federal states. b) Calculated infection pressure at the end of the simulation. Note change in scale bar for each country. c) The number of repeated infections calculated in the model highlights the most affected regions and shows how elevated infection pressures (Figure 2b) continue to generate model infections.

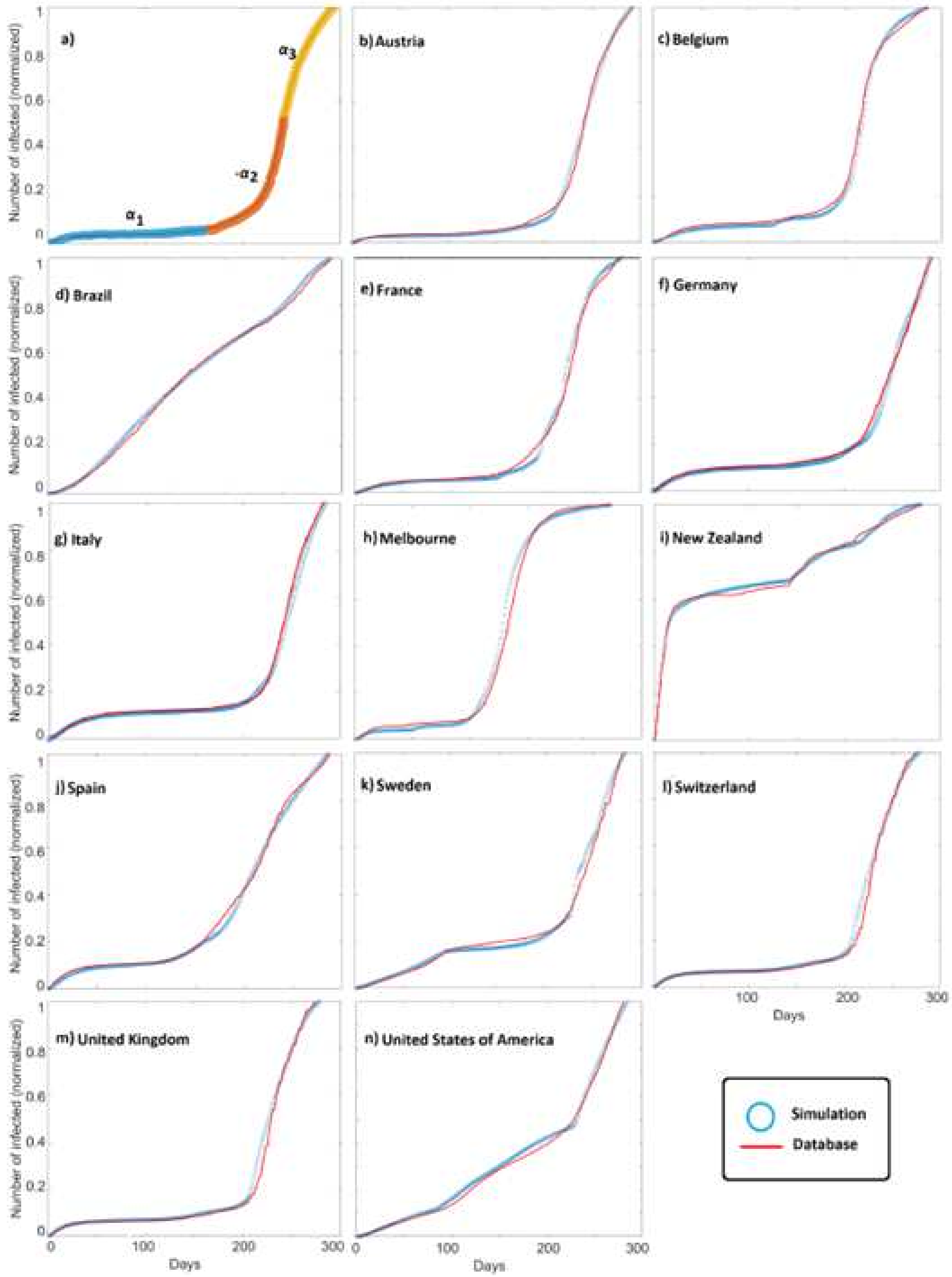

Figure 3

Comparison of data and model results for all data in Figure 1. The determination of ±α is constrained by the data and demonstrated in Figure 3a.

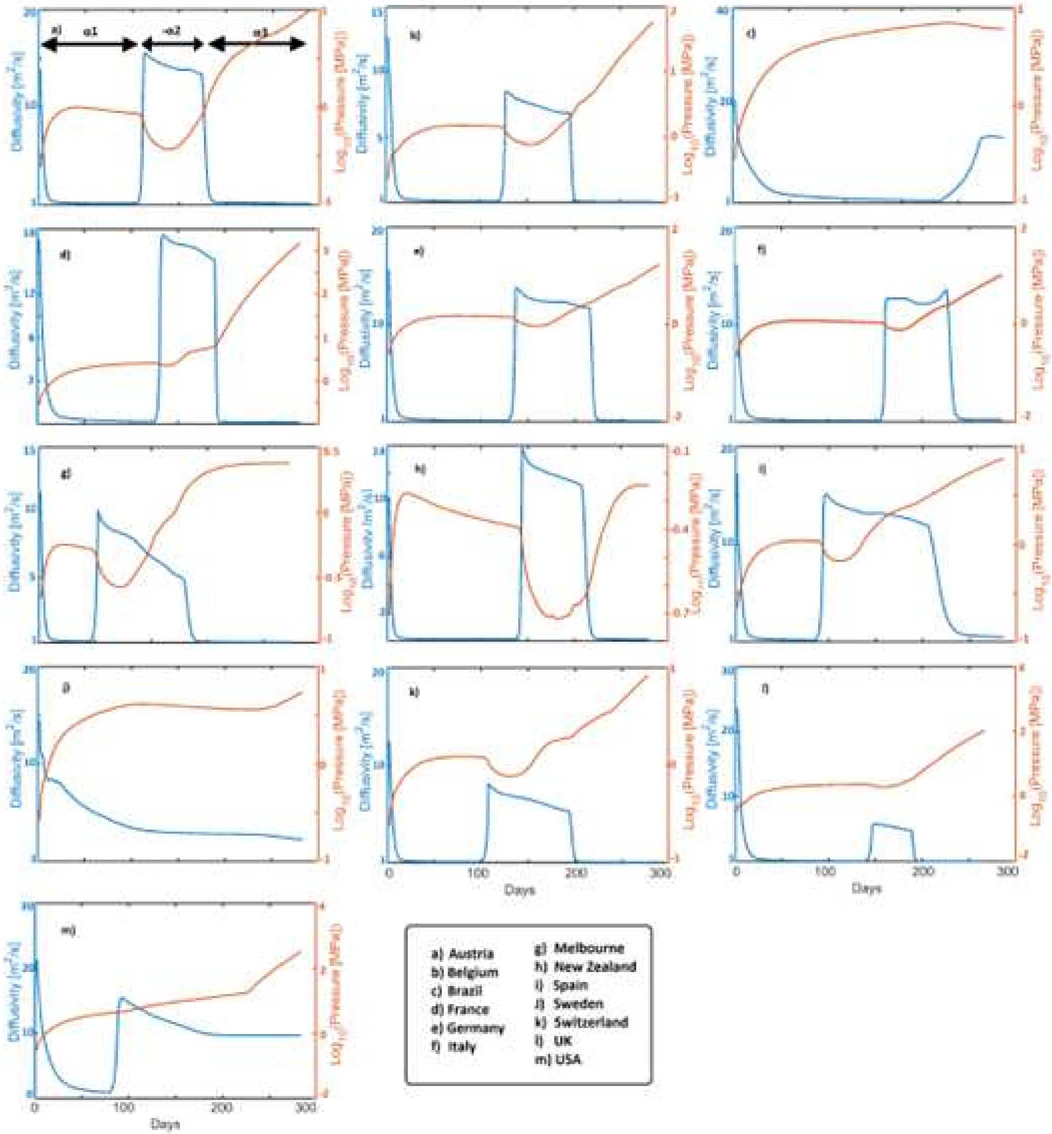

Figure 4

Modelled diffusivity and pressure time histories for triggered infection sites for each individual country and Melbourne.

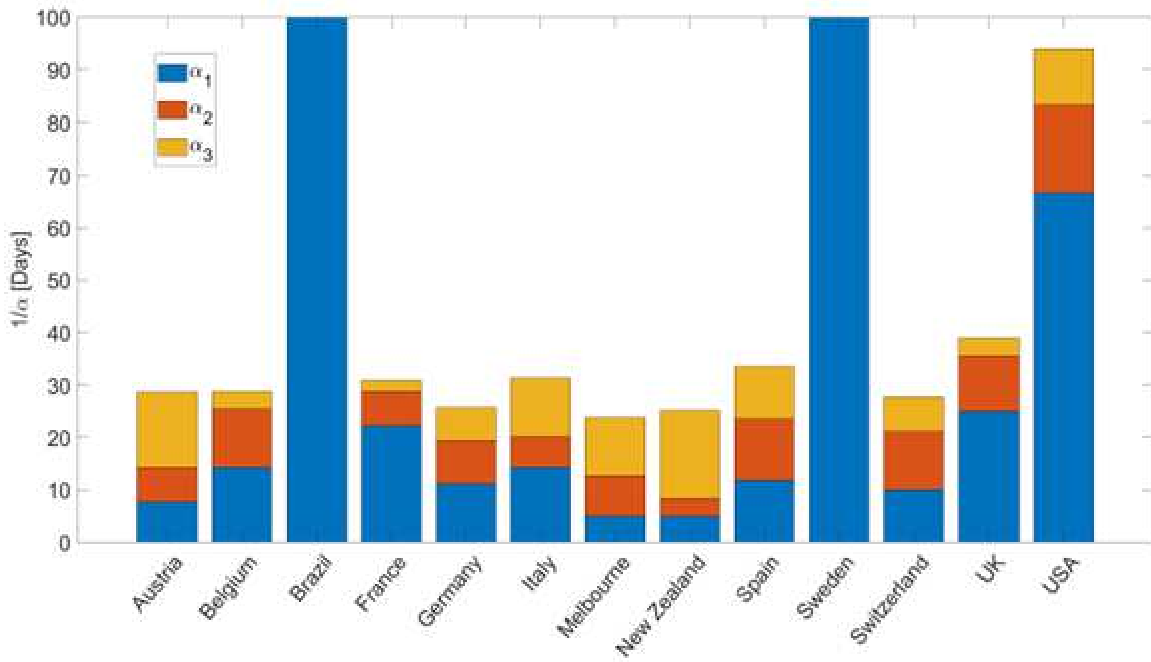

Figure 5

Summary of α values used in the simulations (See Figure 3a) showing long (initial) recovery times (α1) for countries with few initial mitigation measures (e.g. Brazil, Sweden, USA), and to some extent France and the UK. All other countries and Melbourne show similar recovery times in response to swift and similar mitigation measures.

Supplementary Files

This is a list of supplementary files associated with this preprint. Click to download.

- GunatilakeMillerSupplemental.pdf